Supporting Information

N-doped carbon nanotubes encapsulated with FeNi nanoparticles derived from defect-rich, molecule-doped 3D g-C_3N_4 as efficiently bifunctional electrocatalyst for rechargeable zinc-air batteries

Jiahui zheng[a#], Taijia Kang[a#], Bei Liu[a], Pu Wang [a]*, Huaming Li[a], Mei Yang[a,b]*

[a] College of Chemistry, Xiangtan University, Xiangtan 411105, Hunan Province, P. R. China.

[b] Key Lab of Environment-Friendly Chemistry and Application in Ministry of Education, Key Laboratory of Polymeric Materials & Application Technology of Hunan Province, Key Laboratory of Advanced Functional Polymeric Materials of College of Hunan Province, Xiangtan University, Xiangtan 411105, Hunan Province, P. R. China.

* Corresponding authors

Tel.: +86 731 58298572; Fax: +86 731 58293264.

E-mail address: 90wangpu@xtu.edu.cn (P. Wang), yangmei@xtu.edu.cn (M. Yang).

Experimental Section

1. Materials

Hydrochloric acid, melamine, iron(III) nitrate, and nickel(II) nitrate were purchased from Shanghai Aladdin Bio-Chem Technology Co., malazide were purchased from Shanghai Macklin Biochemical Co., Ltd. All the chemicals were analytical agent grade and used as received.

2. Optimization of synthetic conditions for FeNi/N-CNT electrocatalyst

2.1 Optimization of pyrolysis temperature

Firstly, malazide (50 mg) and melamine (4.0 g) were mixed and thoroughly grounded, and then pyrolyzed at 550 ^{o}C for 4 h in N_2 atmosphere with the heating rate of 5 ^{o}C min^{-1}. After cooling down to ambient temperature, the as-obtained brown powder was denoted as D-g-C_3N_4. Secondly, D-g-C_3N_4, $Fe(NO_3)_3 \cdot 9H_2O$ (hereafter denoted as $Fe(NO_3)_3$) and $Ni(NO_3)_2 \cdot 6H_2O$ (hereafter denoted as $Ni(NO_3)_2$) were mixed and thoroughly grounded. The molar ratio of Fe/Ni is 1/1. And then subjected to a carbonization (900−1100 ^{o}C/2 h) under N_2 blowing conditions. The resultant FeNi/N-codoped carbon nanotube was referred as FeNi/N-CNT-x, where x (x = 900, 1000, or 1100) stands for the annealing temperatures.

2.2 Optimization of Fe/Ni molar ratio

The synthesis procedures were identical to that of FeNi/N-CNT-1000 electocatalyst noted in **Section 2.1** except at different Fe/Ni molar ratios. *D*-g-C_3N_4, $Fe(NO_3)_3$ and $Ni(NO_3)_2$ were mixed and thoroughly grounded, in which the Fe/Ni molar ratio was varied from 1/2, 1/1, to

2/1. And then subjected to a carbonization (1000 ºC/2 h) under N_2 blowing conditions. The resulting FeNi/N-CNT electocatalysts were denoted FeNi/N-CNT-1000-1/2, FeNi/N-CNT-1000-1/1, and FeNi/N-CNT-1000-2/1, respectively.

3. Control samples

For comparison, several control samples were also prepared via pyrolysis under identical conditions. They were the *D*-g-C_3N_4 (in the absence of metal salts), *D*-g-C_3N_4/$Fe(NO_3)_3$ (no introduction of $Ni(NO_3)_2$), and *D*-g-C_3N_4/$Ni(NO_3)_2$ (no introduction of $Fe(NO_3)_3$) mixtures. The resulting products are referred to as N-C, Fe/N-C, and Ni/N-C, respectively.

4. Acid-etching and SCN^--poisoning experiments

4.1 Synthesis of E-CN reference electrocatalyst

As HNO_3-etching of FeNi/N-CNT electrocatalyst can remove not only FeNi nanoparticles and M-N_x species, but also N-C configurations, HNO_3-etching was thus performed under harsh conditions. Specifically, FeNi/N-CNT electrocatalyst (50 mg) was dispersed in 60 mL of HNO_3 aqueous solution (9.0 M). The suspension was then stirred at 120 °C, in which the etching time was prolonged until the ORR activity remained unchanged. The obtained electrocatalyst was filtered, washed, and repyrolyzed at 1000 °C for 2 h under N_2 blowing conditions. The HNO_3-etched FeNi/N-CNT electrocatalyst were referred to as E-CN. which was used as the reference electrocatalyst to scrutinize the ORR and OER contributions of N-C configurations.

4.2 HCl-etching of FeNi/N-CNT electrocatalyst

The FeNi/N-CNT electrocatalyst (5.0 mg) was dispersed in 20 mL of HCl aqueous solution (1.0 M). The suspension was stirred at 80 °C for 12 h, after which the suspension /was filtered and washed thoroughly with water.

4.3 SCN^--poisoning of FeNi/N-CNT electrocatalyst

The FeNi/N-CNT electrocatalyst (5.0 mg) was dispersed in 20 mL of KSCN aqueous solution (50 mM). The suspension was stirred at room temperature for 24 h, after which the suspension was filtered and washed thoroughly with water. The SCN^--poisoned FeNi/N-CNT electrocatalyst (denoted FeNi/N-CNT/SCN^-) was obtained after vacuum drying.

4.4 SCN^--poisoning of FeNi/N-CNT/HCl electrocatalyst

The poisoning procedure was similar to that of FeNi/N-CNT/SCN^- electocatalyst, in which the FeNi/N-CNT electrocatalyst was replaced by FeNi/N-CNT/HCl electrocatalyst. The SCN^--poisoned FeNi/N-CNT/HCl electrocatalyst was denoted FeNi/N-CNT/H/SCN^-.

5. Characterization

Fourier transform infrared (FTIR) spectra were acquired on Nicolet 650 spectrophotometer. The N_2 sorption were measured at 77.3 K using Micromeritics TriStar II 3020 surface area and porosimeter analyzer. The specific surface area was calculated using Brunauer-Emmett-Teller (BET) method. The pore size distribution (PSD) was calculated from the adsorption branches of the isotherms using the DFT model. Scanning electron microscopy

(SEM) imaging was performed using S-4800 (JEOL) operated at an acceleration voltage of 10 kV. Transmission electron microscopy (TEM), HRTEM and EDX-mapping were carried out using a Thermo Fischer Talos F200x transmission electron microscope (Japan) operating at 200 kV. Powder X-ray diffraction (XRD) was conducted on a Rigaku D/Max 2500PC diffractometer. Raman spectra were recorded using a Renishaw inVia Raman spectrometer at 25 °C. The Xray photoelectron spectroscopy (XPS) was performed on a K-Alpha 1063 photoelectron spectrometer (Thermo Fisher Scientific, England) with Al-Kα X-ray radiation as the X-ray source for excitation. Thermal gravimetric analysis (TGA) was done using SDT Q600 with a heating rate of 5 ^{o}C min^{-1} under N_2 protection.

6. Electrochemical Measurements

The electrochemical experiments were conducted on a CHI760D electrochemical workstation (Chenhua Instruments Co., Shanghai) in a three-electrode system at 25 °C. A rotating disk electrode (RDE) (diameter: 5 mm) or rotating ring-disk electrode (RRDE) (diameter: 5.6 mm), an Ag/AgCl electrode (3 M KCl), and a platinum coil were used as the working, reference, counter electrodes, respectively, in alkaline electrolyte. The fabrication of working electrode was carried out as follows. Taking FeNi/N-CNT as an example, 2.0 mg catalyst was firstly dispersed in a mixed solution of water (785 μL), ethanol (200 μL), and 15 μL Nafion solution (5.0 wt%), followed by sonication for 0.5 h to form a relatively homogeneous suspension. The effective mass loading on glassy carbon disk electrode was ~0.4 mg cm^{-2}. The same method was used to prepare Pt/C yet the effective mass loading on glassy carbon disk electrode was ~0.1 mg cm^{-2}. In the RDE, the OER performance was examined

from polarization curves obtained using linear scanning voltammetry (LSV) at 10 mV s^{-1} in 0.1 M KOH under saturated O_2 to provide the O_2/H_2O equilibrium at 1.23 V versus reversible hydrogen electrode (RHE). The ORR activity was evaluated by LSV on RDE in an O_2-saturated 0.1 M KOH solution by flowing O_2 with a varied rotating speed from 400 to 2000 rpm at a rate of 10 mV s^{-1}. All measured potentials in this study were converted to RHE according to the following equation:

$$E_{(RHE)} = E_{Ag/AgCl} + 0.210 + 0.059 \times pH$$

The electron transfer number (n) per oxygen molecule involved in the typical ORR process was calculated from the slopes of Koutecky-Levich (K-L) equation:

$$1/J = 1/J_L + 1/J_K = 1/(B\omega^{1/2}) + 1/J_K$$

$$B = 0.2nFC_0(D_0)^{2/3}v^{-1/6}$$

where J, J_L, J_k are the measured current density, diffusion current density, and kinetic current density, respectively. ω is the electrode rotating speed in rpm, F is the Faraday constant (96485 C mol^{-1}), D_0 is the diffusion coefficient of oxygen in 0.1 M KOH (1.9×10^{-5} cm^2 s^{-1}), v is the kinetic viscosity (0.01 cm^2 s^{-1}), and C_0 is the bulk concentration of oxygen (1.2×10^{-6} mol cm^{-3}). The constant 0.2 is adopted when the rotation speed is expressed in rpm.

The RRDE measurements were also conducted to determine peroxide species formed and the electron transfer number (n). The ring-disk electrode was scanned at a rate of 10 mV s^{-1} and the ring electrode potential in the RRDE system was set to 1.4 V versus RHE. The yield of peroxide species (%HO_2^- in alkaline media) and n were calculated by the following equations:

$$OH_2^-\% = 200 \times \frac{i_r/N}{i_r/N + i_d}$$

$$n = 4 \times \frac{i_d}{i_r/N + i_d}$$

where i_d and i_r are the disk and ring currents, respectively. N is current collection efficiency of Pt ring, which was determined to be 0.37.

7. Assembly of Zn-air Batteries

Liquid Zn-air batteries were assembled to access the battery performance. The catalyst inks were prepared as discussed in abovementioned electrochemical measurements, which were uniformly drop-cast onto gas diffusion layer (GDL) carbon paper with catalyst loading of 1.50 mg cm^{-2}. Rechargeable Zn-air batteries using a mixed Pt/C (20 wt %, JM) and IrO_2 (99.9%) (the mass ratio of Pt/C : IrO_2 = 1:1; Pt/C + IrO_2 loadings = 1.0 mg cm^{-2}) as air-cathode was also assembled for comaprison. The reaction area of cathode is 1 cm^2. Polished zinc foil was chosen as anode in an electrolyte containing 6 M KOH and 0.2 M $Zn(OAc)_2$.

8. DFT calculations

The spin polarized first principle DFT calculations are performed by Vienna Ab initio Simulation Package(VASP) with the projector augmented wave (PAW) method [1]. The exchange-functional is treated using the generalized gradient approximation (GGA) of Perdew-Burke-Ernzerhof (PBE) [2] functional. The energy cutoff for the plane wave basis expansion was set to 450 eV and the force on each atom less than 0.02 eV/Å was set for convergence criterion of geometry relaxation. The current work employs the metallic (6, 6) carbon nanotube (CNT). At least 10 Å vacuum layer are exposed to the direction perpendicular to the CNT axis. Brillouin-zone integration was sampled by 1×1×3 k-point sampling for geometry

optimization and 1×1×7 k-point sampling for the calculation of density of states (DOS). The self-consistent calculations apply a convergence energy threshold of 10^{-5} eV. The DFT-D3 method was employed to consider the van der Waals interaction [3].

The general equation for the ORR reaction can be written as:

$$2H_2O(l) + O_2(g) + 4e^- \rightarrow 4OH^-$$

The ORR process we studied for bimental model is mainly a four-electron process. We believe that the ORR reaction process is mainly the following five steps, which are listed as below:

$$\text{Step 1: } * + O_2(g) \rightleftarrows 2{}^*O$$

$$\text{Step 2: } 2{}^*O + e^- + H_2O(l) \rightleftarrows {}^*OOH + OH^-$$

$$\text{Step 3: } {}^*OOH + e^- \rightleftarrows {}^*O + OH^-$$

$$\text{Step 4: } {}^*O + e^- + H_2O(l) \rightleftarrows {}^*OH + OH^-$$

$$\text{Step 5: } {}^*OH + e^- \rightleftarrows OH^- + *$$

And the OER reaction occurs inversely from step 5 to step 1.

Figures and Tables

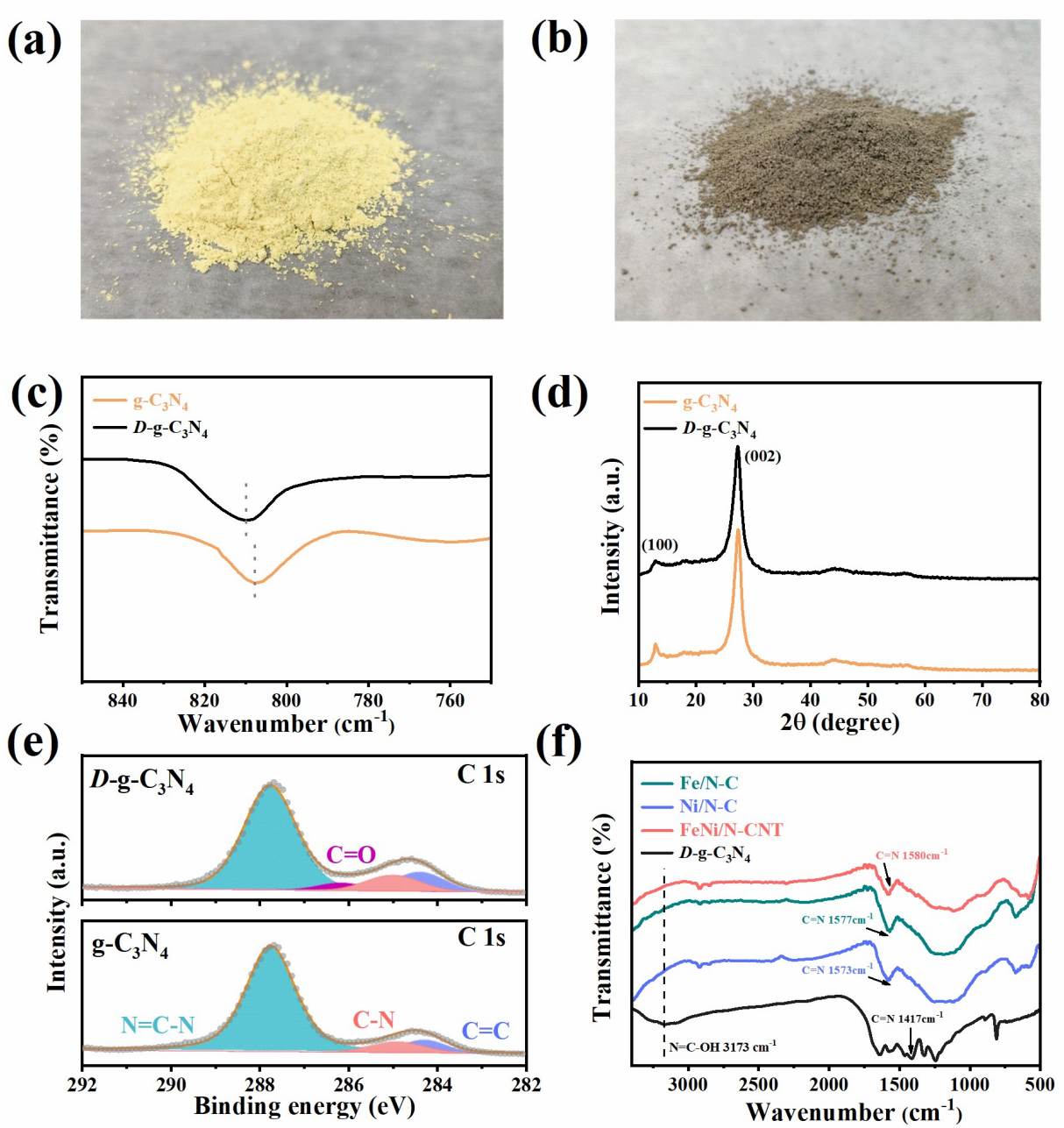

Figure S1. Photographs for (a) g-C_3N_4 and (b) *D*-g-C_3N_4, (c) FTIR spectra of *D*-g-C_3N_4 and g-C_3N_4, (d) XRD patterns of *D*-g-C_3N_4 and g-C_3N_4, (e) XPS C 1s spectra for *D*-g-C_3N_4 and g-C_3N_4, (f) FTIR spectra of Fe/N-C, Ni/N-C, FeNi/N-CNT and *D*-g-C_3N_4.

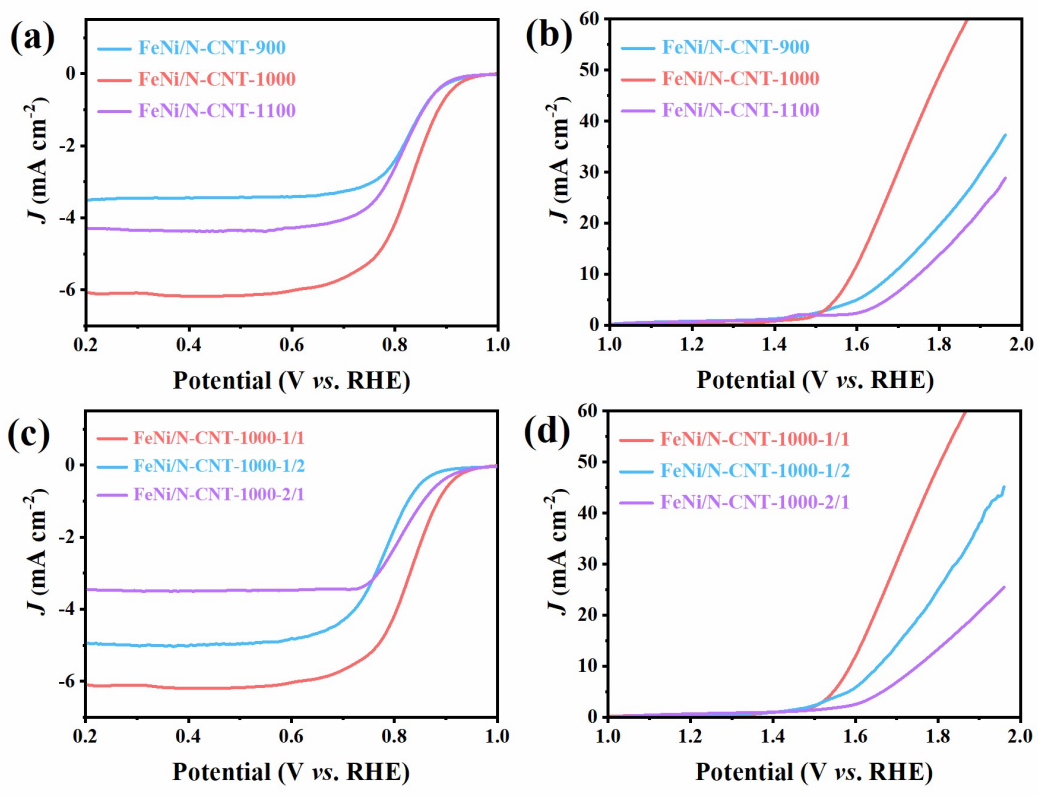

Figure S2. (a) ORR and (b) OER performance of FeNi/N-CNT-900, FeNi/N-CNT-1000, and FeNi/N-CNT-1100 electrocatalysts, and 900/1000/1100 denoted the different pyrolysis temperature. (c) ORR and (d) OER performance of FeNi/N-CNT-1000-1/1, FeNi/N-CNT-1000-1/2, and FeNi/N-CNT-1000-2/1 electrocatalysts, and 1/1, 1/2, 2/1 denoted the different Fe/Ni ratios.

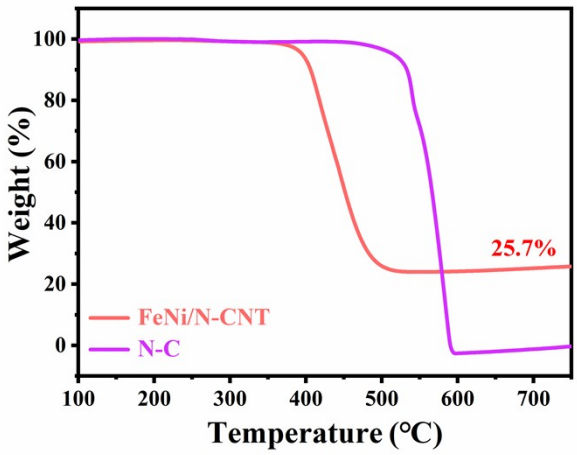

Figure S3. TGA curves of FeNi/N-CNT and N-C electrocatalysts.

Table S1. C, N, O, Fe, and Ni contents of the as-synthesized electrocatalysts.

Catalysts	ICP (wt.%)		XPS									
			Elemental Content (at.%)					N Configuration (%)				
	Fe	Ni	C	O	N	Fe	Ni	Pyridinic-N	Graphitic-N	M-N_x	Pyrrolic-N	Oxidized-N
FeNi/N-CNT	6.47	6.63	88.04	3.44	6.93	0.77	0.83	22.18	31.46	12.81	14.24	19.31

Notes: FeNi/N-CNT (alloyed FeNi nanoparticles encapsulated within N-doped carbon nanotube).

Table S2. Content comparison of different Raman peaks fitted using Gaussian peaks.

Samples	Type of Raman peak				
	I (%)	*D* (%)	*D*' (%)	*G* (%)	$Area_D/Area_G$
FeNi/N-CNT-900	9.55	41.49	17.75	31.21	1.33
FeNi/N-CNT-1000	8.56	36.53	21.66	33.25	1.10
FeNi/N-CNT-1100	10.59	33.00	25.51	30.90	1.07

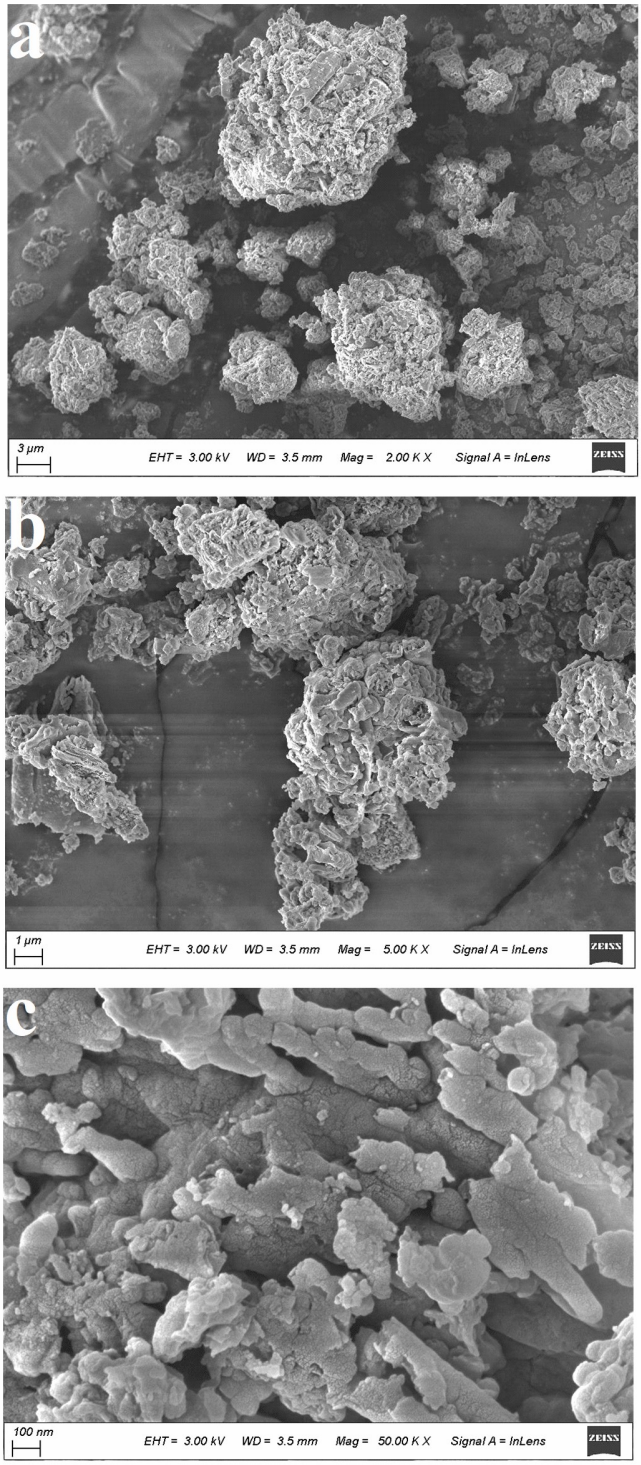

Figure S4. (a-c) SEM images of the precursor *D*-g-C_3N_4.

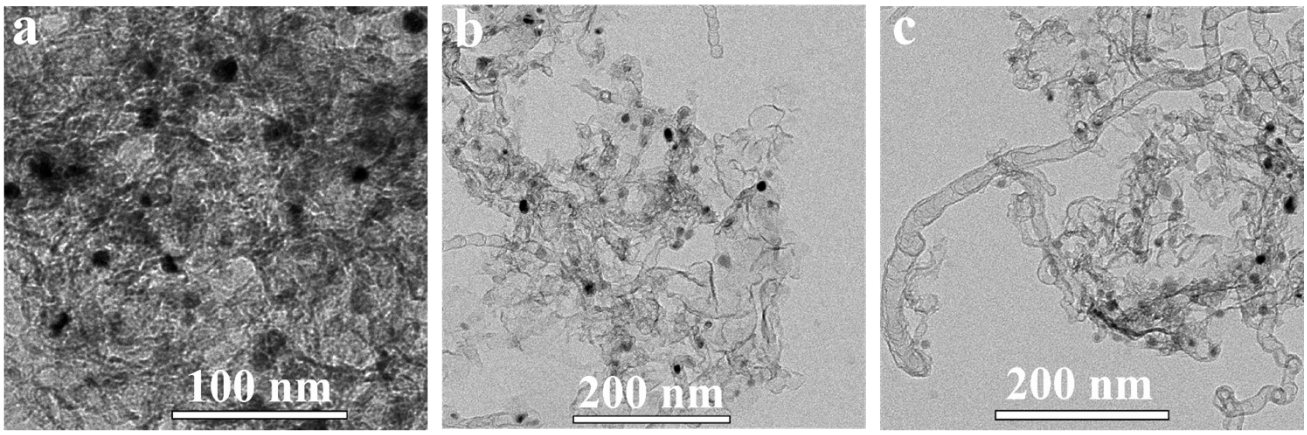

Figure S5. The generative process of FeNi/N-CNT. TEM images recorded at (a) at 500-550 °C, (b) at 650-800 °C, and (c) at 800-1000 °C.

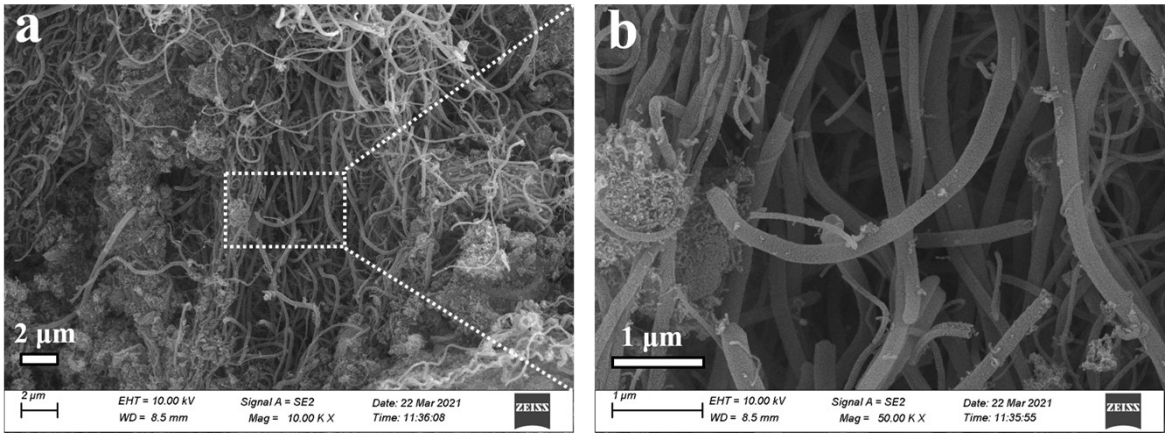

Figure S6. SEM images of the FeNi/N-CNT.

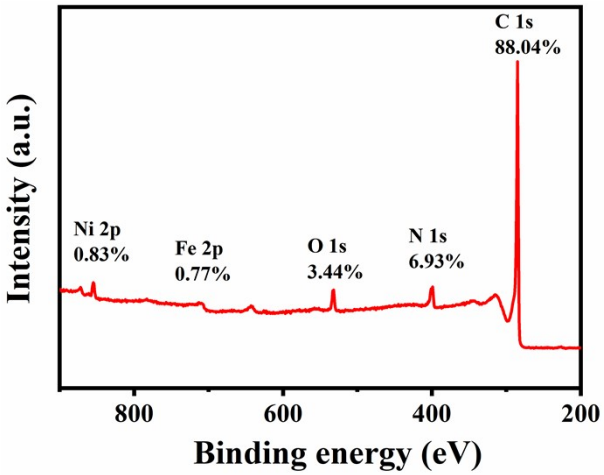

Figure S7. Full-scan XPS spectrum of the FeNi/N-CNT electrocatalyst.

Table S3. The specific surface areas (S_{BET}) and total pore volumes (V_t) of the as-synthesized electrocatalysts.

Electrocatalysts	S_{BET} (m^2 g^{-1})			V_t (cm^3 g^{-1})		
	Total	Micro	External	Total	Micro	External
FeNi/N-CNT-900	334.8	66.8	268.0	0.80	0.04	0.76
FeNi/N-CNT-1000	270.6	23.0	247.6	1.04	0.01	1.03
FeNi/N-CNT-1100	105.8	1.4	104.4	0.442	0.002	0.440

Table S4. ORR and OER activities of the as-synthesized electrocatalysts.

Catalysts	ORR			OER	ΔE
	E_o (V *vs*. RHE)	$E_{1/2}$ (V *vs*. RHE)	J_l (mA cm^{-2})	$E_{j=10}$ (V *vs*. RHE)	
FeNi/N-CNT	0.975	0.830	6.02	1.587	0.757
Fe/N-C	0.935	0.809	4.37	1.774	0.965
Ni/N-C	0.916	0.801	5.06	1.733	0.932
N-C	0.857	0.761	4.84	1.875	1.114
Pt/C	0.965	0.835	5.26	N/A	0.765
IrO_2	N/A	N/A	N/A	1.60	

As for the FeNi/N-CNT electrocatalyst, it is plausible to assume that the active sites for both ORR and OER primarily involve FeNi nanoparticles, M-N_x species (i.e., Fe-N_x and Ni-N_x), and N-C configurations (i.e., pyridinic-N and graphitic-N). In order to quantify their respective ORR contributions, the FeNi/N-CNT electrocatalyst was washed with 1.0 M HCl aqueous solution, during which FeNi nanoparticles were completely removed yet the M-N_x sites were retained, as revealed by XRD study (**Figure S9**). In other words, the ORR active sites in the

HCl-treated electrocatalyst (denoted FeNi/N-CNT/HCl) are M-N_x species and N-C configurations. To assess the ORR contribution of N-C configurations, the E-CN reference electrocatalyst was used, in which the ORR was solely resulted from the N-C configurations. In this context, the relative contributions of the FeNi nanoparticles, M-N_x species, and N-C configurations to the ORR in the FeNi/N-CNT electrocatalyst were estimated by using $\Delta E_{1/2}$ value, as discussed in the main text.

By comparing FeNi/N-CNT ($E_{1/2}$ = 830 mV) with E-CN reference electrocatalyst ($E_{1/2}$ = 482 mV), a negative $E_{1/2}$ shift of 348 mV ($\Delta E_{1/2}$ = 830 − 482 = 348 mV) was observed, revealing that the total ORR contributions of the FeNi nanoparticles, M-N_x species, and N-C configurations are approximately 348 mV. Thus, the contributions of FeNi nanoparticles, M-N_x species, and N-C configurations to the ORR can be assessed by the $\Delta E_{1/2}$ values via comparing the differences between FeNi/N-CNT ($E_{1/2}$ = 830 mV) and FeNi/N-CNT/HCl ($E_{1/2}$ = 807 mV; thus $\Delta E_{1/2}$ = 830 − 807 = 23 mV), between FeNi/N-CNT/HCl ($E_{1/2}$ = 807 mV) and N-C ($E_{1/2}$ = 761 mV; thus $\Delta E_{1/2}$ = 807 − 761 = 46 mV), and between N-C ($E_{1/2}$ = 761 mV) and E-CN ($E_{1/2}$ = 482 mV; thus $\Delta E_{1/2}$ = 761 − 482 = 279 mV), yielding 6.60% (= 23 mV/348 mV), 13.22% (= 46 mV/348 mV), and 80.18% (= 279 mV/348 mV), respectively. It should be noted that this was a rough estimation and did not take into account the differences between porosities (i.e., S_{BET} and V_t) and/or N-doping (i.e., N-C configurations and their relative contents) in the FeNi/N-CNT and N-C as well as E-CN reference electrocatalysts.

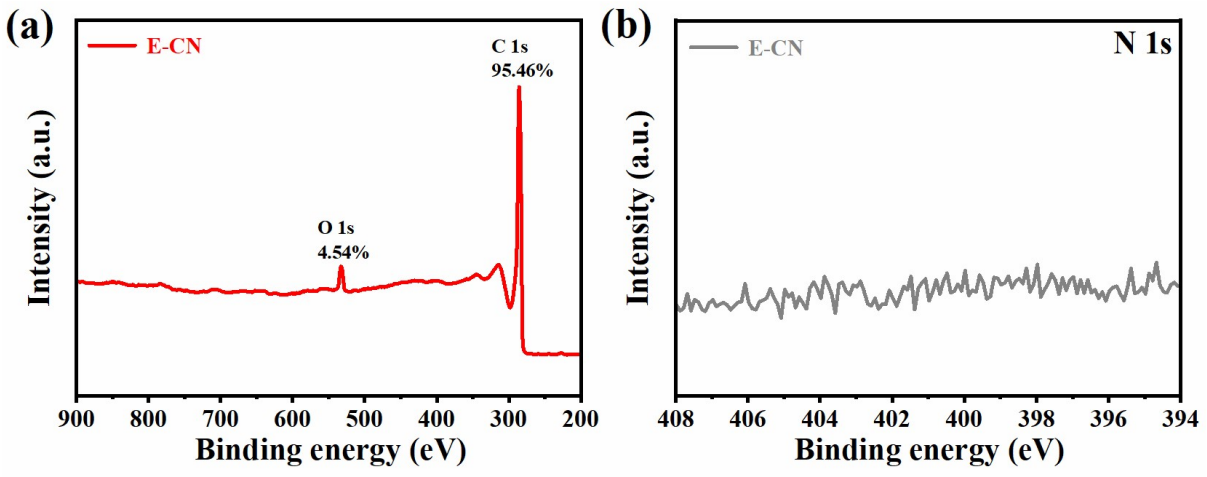

Figure S8. (a) Full-scan XPS spectrum and (b) N 1s spectra for the E-CN electrocatalyst.

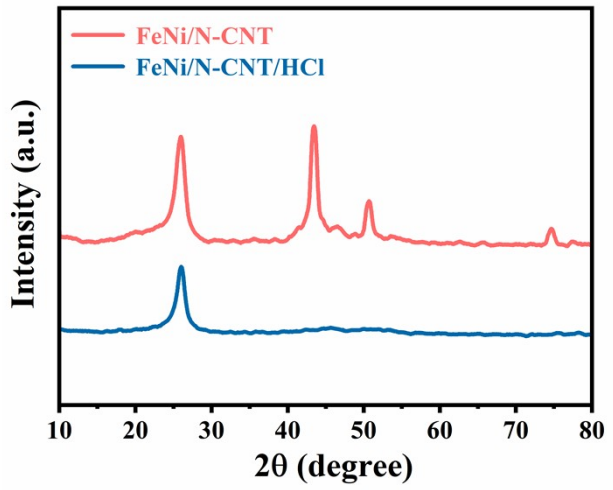

Figure S9. XRD patterns of FeNi/N-CNT and FeNi/N-CNT/HCl (see **section 4.2** in Experimental Section for detailed sample preparation) electrocatalysts.

To further demonstrate the ORR contribution of M-N_x sites, the SCN^--poisoning experiments were conducted on both FeNi/N-CNT and FeNi/N-CNT/HCl electrocatalysts due to the fact that SCN^- can block the M-N_x active sites. **Figure S10a** shows LSV curves of FeNi/N-CNT/SCN^- and FeNi/N-CNT/H/SCN^- lectrocatalysts in O_2-saturated 0.1 M KOH solution at 1600 rpm. The comparison between the FeNi/N-CNT ($E_{1/2}$ = 830 mV) and FeNi/N-CNT/SCN^- ($E_{1/2}$ = 782 mV) elctrocatalysts yielded a $\Delta E_{1/2}$ of 48 mV ($\Delta E_{1/2}$ = 830 − 782 = 48 mV) for FeNi/N-CNT/SCN^- electrocatalyst (**Figure S10b**). Similarly, a $\Delta E_{1/2}$ of 53 mV ($\Delta E_{1/2}$

= 807 − 754 = 53 mv) was observed for the FeNi/N-CNT/H/SCN⁻ electrocatalyst (**Figure S10b**) by comparing the FeNi/N-CNT/HCl ($E_{1/2}$ = 807 mv) with the FeNi/N-CNT/H/SCN⁻ ($E_{1/2}$ = 754 mV). Taken together, these results confirmed that the realtive contribution of M-N_x sites to the ORR is around 13.79% (= 48 mV/348 mV) or 15.23% (= 53 mV/348 mV) in the FeNi/N-CNT electrocatalyst, approaching 13.22% as discussed above.

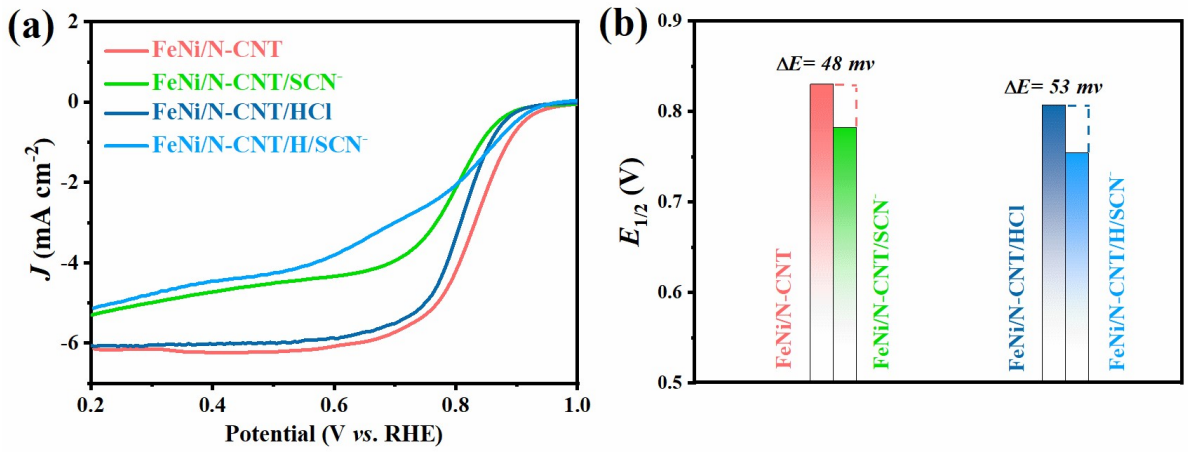

Figure S10. (a) LSVs of FeNi/N-CNT, FeNi/N-CNT/SCN⁻, FeNi/N-CNT/HCl and FeNi/N-CNT/H/SCN⁻ lectrocatalysts in O_2-saturated 0.1 M KOH solution at 1600 rpm (see **Section 4.3** and **4.4** in Supporting Information for detailed sample preparation). (b) The relative contributions of M-N_x sites to the ORR estimated by using $E_{1/2}$ value as the criterion.

Likewise, the relative contributions of FeNi nanoparticles, M-N_x species, and N-C configurations to the OER were also investigated by using $E_{j=10}$ as the criterion. The $E_{j=10}$ values measured for the FeNi/N-CNT, FeNi/N-CNT/HCl, and N-C electrocatalysts as well as E-CN reference electrocatalyst are 1.587 V, 1.747 V, 1.875 V, and 1.940 V, respectively. The $\Delta E_{j=10}$ values between E-CN and N-C, N-C and FeNi/N-CNT/HCl, FeNi/N-CNT/HCl and FeNi/N-CNT, and E-CN and FeNi/N-CNT electrocatalysts are 65 mV, 128 mV, 160 mV, and

353 mV, respectively. Thus, the relative contributions of N-C configurations, M-N_x species, and FeNi nanoparticles are 65 mV, 128 mV, 160 mV, respectively, in the FeNi/N-CNT electrocatalyst, accounting for 18.41% (= 65 mV/353 mV), 36.26% (= 128 mV/353 mV), 45.33% (= 160 mV/353 mV), respectively. It is also notable that such a rough estimation did not take into account the differences between porosities (i.e., SBET and Vt) and/or N-doping (i.e., N-C configurations and their relative contents) in the FeNi/N-CNT and N-C as well as E-CN reference electrocatalysts.

To further demonstrate the relative contribution of M-N_x sites, SCN^--poisoning experiments were conducted on both FeNi/N-CNT and FeNi/N-CNT/HCl electrocatalysts. **Figure S11a** shows the OER polarization curves of FeNi/N-CNT/SCN^- and FeNi/N-CNT/H/SCN^- catalysts in O_2-saturated 0.1 M KOH solution. The $\Delta E_{j=10}$ values between FeNi/N-CNT/SCN^- and FeNi/N-CNT, and FeNi/N-CNT/H/SCN^- and FeNi/N-CNT/HCl are 124 mV and 108 mV, respectively, which are almost the same to each other (**Figure S11b**). These results further confirmed that the relative contribution of M-N_x sites to OER is approximately 36.26% in the FeNi/N-CNT electrocatalyst.

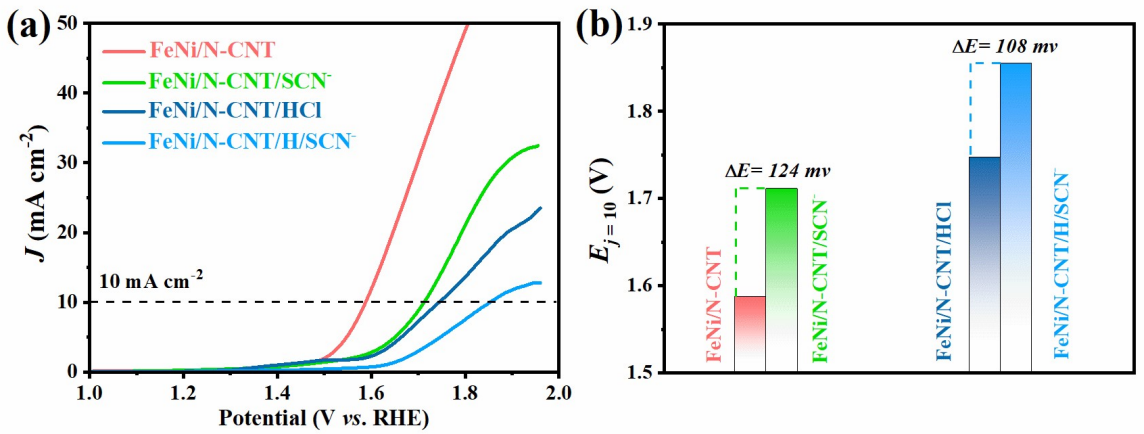

Figure S11. (a) OER polarization curves of FeNi/N-CNT, FeNi/N-CNT/SCN^-, FeNi/N-CNT/HCl and FeNi/N-CNT/H/SCN^- electrocatalysts in O_2-saturated 0.1 M KOH solution (see **Section 4.3** and **4.4** in Supporting Information for detailed sample preparation). (b) The relative contribution of M-N_x sites to the OER estimated by using $E_{j=10}$ value as the criterion.

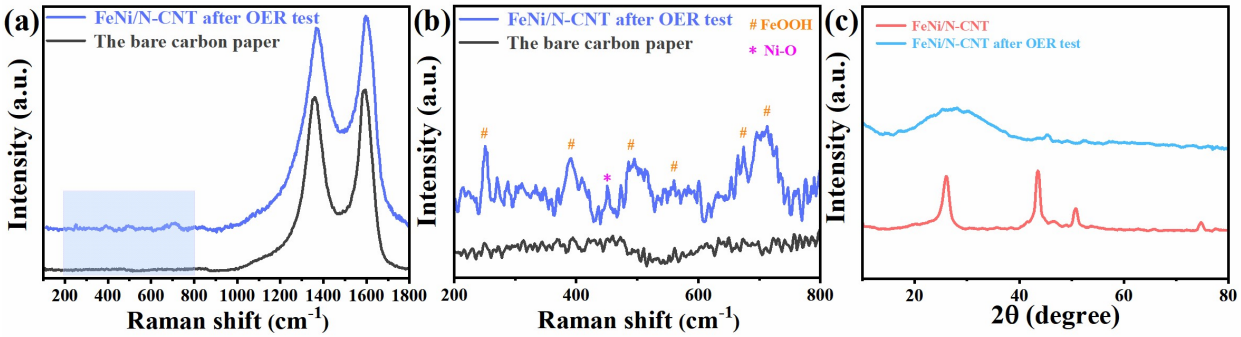

Figure S12. (a) Raman spectra of FeNi/N-CNT after OER test and the bare carbon paper, (b) zoom-in view of (a) in 200-800 cm^{-1} region. (c) XRD patterns of FeNi/N-CNT after OER test and FeNi/N-CNT.

To verify the generation of $Ni_{1-x}Fe_xOOH$ species (after the OER process) more accurately, Raman testing was then conducted and the corresponding results are shown in **Figure S12**. The peaks corresponding to $Ni_{1-x}Fe_xOOH$ in that of FeNi/N-CNT are relatively small in intensity due to the limited amount of $Ni_{1-x}Fe_xOOH$ on the shell of nanotube [4-7]. For this reason, no $Ni_{1-x}Fe_xOOH$ signal can be detected within the analytical range of the XRD technique.

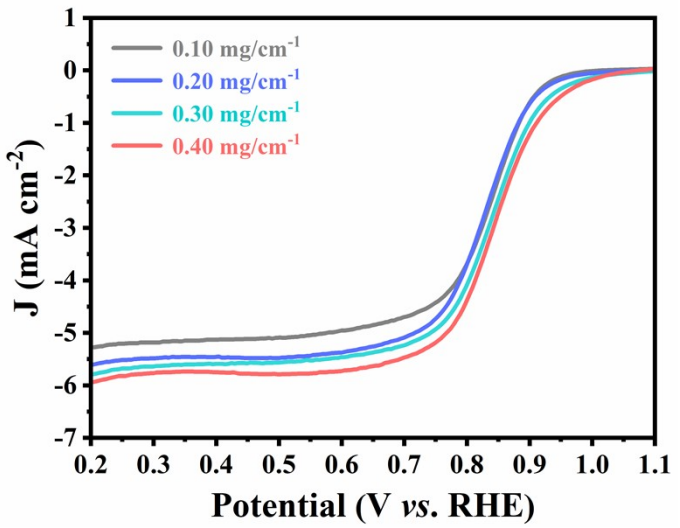

Figure S13. LSV curves of the Pt/C with different loadings (0.1 mg cm^{-2} to 0.4 mg cm^{-2}) in O_2-saturated 0.1 M KOH solution at 1600 rpm.

Table S5. Comparison of the performances of FeNi/N-CNT electrocatalysts for ORR/OER and rechargeable Zn-air battery with those based on monometallic or bimetallic M/N-C electrocatalysts reported in literature.

Catalysts	$E_{1/2}$	$E_{j=10}$	ΔE	Power density (mW cm^{-2})	Stability	Ref.
FeNi/N-CNT	**0.830**	**1.587**	**0.757**	**127.0**	**800 h @ 5 mA cm^{-2}**	**This work**
3D Fe/N-G#4	0.852	1.62	0.770	168.2	60 h @ 20 mA cm^{-2}	8
CoS_x/Co-NC-800	0.800	1.54	0.740	103.0	90 h @ 5 mA cm^{-2}	9
NiFe/N-CNT	0.750	1.52	0.770	300.7	100 h @ 5 mA cm^{-2}	10
NiFe@NCx	0.860	1.55	0.690	85.00	34 h @ 10 mA cm^{-2}	11
$Fe_1Co_1S_x$@NSPC	0.820	1.62	0.800	159.0	130 h @ 10 mA cm^{-2}	12
Ni_3Fe/N-C	0.780	1.60	0.820	N/A	420 h @ 10 mA cm^{-2}	13
S,N-Fe/N/C-CNT	0.850	1.60	0.750	102.7	100 h @ 5 mA cm^{-2}	14
Co-N_x/C NRA	0.870	1.53	0.660	193.2	N/A	15
NiFe@N-CFs	0.820	1.53	0.710	102.0	300 h @ 10 mA cm^{-2}	16
FeCo-NC_{ps}	0.845	1.61	0.765	242.0	155 h @ 10 mA cm^{-2}	17
h-FeCo alloy/N-CNFs	0.870	1.56	0.690	N/A	238 h @ 10 mA cm^{-2}	18
Co-N-PHCNTs	0.890	1.62	0.730	125.4	673 h @ 5 mA cm^{-2}	19
FeCo/FeCoNi@NCNTs-HF	0.850	1.60	0.750	156.2	240 h @ 5 mA cm^{-2}	20

Note: All ORR/OER tests were conducted in 0.1 M KOH aqueous solution.

References

[1] P. E. Blöchl, *Phys. Rev. B*, 1994, **50**, 17953-17979.

[2] J. P. Perdew, J. A. Chevary, S. H. Vosko, K. A. Jackson, M. R. Pederson, D. J. Singh and C. Fiolhais, *Phys. Rev. B*, 1992, **46**, 6671.

[3] S. Grimme, J. Antony, S. Ehrlich and H. Krieg, *J. Chem. Phys.*, 2010, **132**, 154104.

[4] L. Cai, J. Zhao, H. Li, J. Park, I.S. Cho, H.S. Han and X. Zheng, *ACS Energy Lett.*, 2016, **1**, 624-632.

[5] L. Wu, L. Yu, B. McElhenny, X. Xing, D. Luo, F. Zhang, J. Bao, S. Chen and Z. Ren, *Appl. Catal. B: Environ.*, 2021, **294**, 120256.

[6] W. D. Chemelewski, H. C. Lee, J. F. Lin, A. J. Bard and C. B. Mullins, *J. Am. Chem. Soc.*, 2014, **136**, 2843-2850.

[7] C. Liang, P. Zou, A. Nairan, Y. Zhang, J. Liu, K. Liu, S. Hu, F. Kang, H. J. Fan and C. Yang, *Energy Environ. Sci.*, 2020, **13**, 86-95.

[8] C. Wang, Z. Li, L. Wang, X. Niu and S. Wang, *ACS Sustainable Chem. Eng.*, 2019, **7**, 13873-13885.

[9] Q. Lu, J. Yu, X. Zou, K. Liao, P. Tan, W. Zhou, M. Ni and Z. Shao, *Adv. Funct. Mater.*, 2019, **29**, 1904481.

[10] H. Lei, Z. Wang, F. Yang, X. Huang, J. Liu, Y. Liang, J. Xie, M. S. Javed, X. Lu and S. Tan, *Nano Energy*, 2020, **68**, 104293.

[11] J. Zhu, M. Xiao, Y. Zhang, Z. Jin, Z. Peng, C. Liu, S. Chen, J. Ge and W. Xing, *ACS Catal.*, 2016, **6**, 6335-6342.

[12] W. Fang, P. Dai, H. Hu, T. Jiang, H. Dong and M. Wu, *Appl. Surf. Sci.*, 2020, **505**, 144212.

[13] G. Fu, Z. Cui, Y. Chen, Y. Li, Y. Tang and J. B. Goodenough, *Adv. Energy Mater.*, 2017, **7**, 1601172.

[14] P. Chen, T. Zhou, L. Xing, K. Xu, Y. Tong, H. Xie, L. Zhang, W. Yan, W. Chu and C. Wu, *Angew. Chem. Int. Ed.*, 2017, **129**, 625-629.

[15] I. S. Amiinu, X. Liu, Z. Pu, W. Li, Q. Li, J. Zhang, H. Tang, H. Zhang and S. Mu, *Adv. Funct. Mater.*, 2018, **28**, 1704638.

[16] Y. Niu, X. Teng, S. Gong and Z. Chen, *J. Mater. Chem. A*, 2020, **8**, 13725-13734.

[17] J. Liu, T. He, Q. Wang, Z. Zhou, Y. Zhang, H. Wu, Q. Li, J. Zheng, Z. Sun, Y. Lei, J. Ma and Y. Zhang, *J. Mater. Chem. A*, 2019, **7**, 12451-12456.

[18] Y. Ma, W. Zang, A. Sumboja, L. Mao, X. Liu, M. Tan, S. Pennycook, Z. Kou, Z. Liu, X. Li and J. Wang, *Sustainable Energy Fuels*, 2020, **4**,1747-1753.

[19] Y. Guan, Y. Li, S. Luo, X. Ren, L. Deng, L. Sun, H. Mi, P. Zhang and J. Liu, *Appl. Catal. B*, 2019, **256**, 117871.

[20] Z. Wang, J. Ang, B. Zhang, Y. Zhang, X. Y. D. Ma, T. Yan, J. Liu, B. Che, Y. Huang and X. Lu, *Appl. Catal. B*, 2019, **254**, 26-36.